

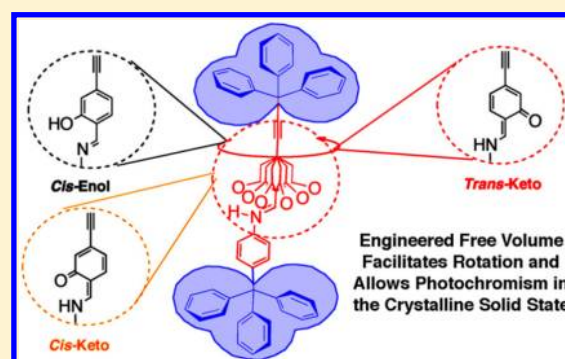
Engineered Photochromism in Crystalline Salicylidene Anilines by Facilitating Rotation to Reach the Colored *trans*-Keto Form

Ira O. Staehle, Braulio Rodríguez-Molina, Saeed I. Khan, and Miguel A. Garcia-Garibay*

Chemistry and Biochemistry Department, University of California, Los Angeles, 90095 United States

Supporting Information

ABSTRACT: The photochromism of crystalline salicylidene anilines regularly occurs by a volume-conserving bicycle pedal motion that transposes the relative position of the two atoms of the central imine bond while leaving the original salicylaldehyde and aniline rings unchanged. Considering the challenges involved in the preparation of packing structures that are conducive to the bicycle pedal process, we tested a design based on a structural strategy that is known to facilitate the rotation of phenyl rings in the solid state, allowing the molecules to be photoreactive. Three salicylidene aniline molecular rotors linked to bulky trityl, tetraphenylmethyl, or pentiptycene stators were prepared and crystallized, and their solid state photochromism was confirmed. In one case, isomorphous crystals of a deuterium labeled deoxo-salicylidene aniline model system were analyzed by solid state ^2H NMR to confirm that the corresponding packing structure is conducive to fast rotation in the solid state.



INTRODUCTION

Photochromism is the reversible transformation of a single chemical species between two states that absorb in different regions of the ultraviolet and visible spectrum.¹ Photochromic molecules are of considerable interest due to their potential use in many new technologies, including nonlinear optics,² information storage,³ sensors,⁴ and molecular machines.⁵ These and other applications require photochromism to operate in solid matter, that is, crystals, polymers, or thin films. For that reason, the solid-state photochromism of an increasing number of compounds like diarylethenes,⁶ spiropyrans,⁷ azobenzenes,^{5,8} and salicylidene anilines⁹ has been explored with increasing interest.

Photochromism generally entails changes in bonding patterns and extent of conjugation resulting from electrocyclic reactions, proton transfer, and tautomerism, as well as *trans*-to-*cis* double bond isomerizations.¹ Photochromism also causes changes in size and shape that are generally not allowed within the rigid environment of a solid matrix. In fact, the detailed nature of the crystalline environment plays a critical role in determining the presence or absence of photochromic behavior for homologous series that consistently display it in solution.¹⁰ For example, out of three polymorphs of *N*-3,5-di-*tert*-butylsalicylidene-3-carboxyaniline, only the α and β forms exhibit photochromism while the structure of the γ form remains unchanged upon exposure to light.¹¹ In the specific case of salicylidene anilines (SAs), they exist in thermal equilibrium between *cis*-enol and *cis*-keto tautomeric forms, as shown in Figure 1, with the aromatic hydroxyl-bearing tautomer being the most stable.

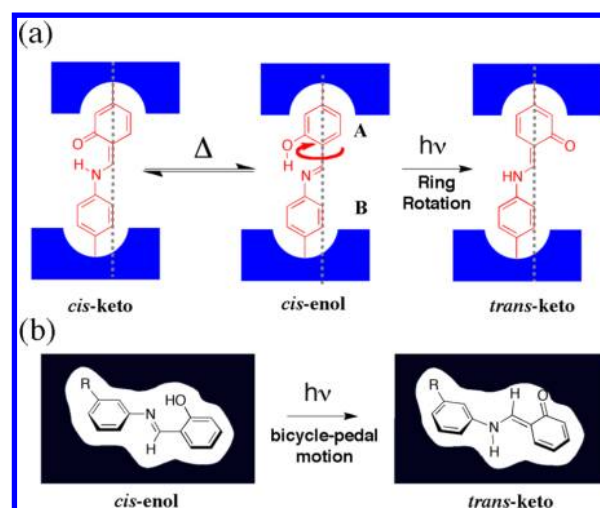


Figure 1. Photochromism of crystalline salicylidene anilines (SA) through (a) hypothetical ring rotation in a crystal-engineered molecular rotor built with a shielding stator that creates free volume for rotation, and (b) by a volume conserving, bicycle-pedal motion in the cavity of a close-packed crystal.

Photochromism in these molecules occurs upon electronic excitation of the stable *cis*-enol followed by an adiabatic oxygen-to-nitrogen proton transfer reaction and an isomerization process that positions the N–H group opposite to the carbonyl oxygen to form the longer-lived, *trans*-keto species,^{1a} which has

Received: May 25, 2014

Published: June 2, 2014

a red colored *ortho*-quino-dimethane chromophore¹² (Figure 1). While the proton-transfer step should not be hindered in a solid state environment, isomerization from the *cis*-enol to the *trans*-keto structure is expected to be difficult, especially in close-packed crystals.¹³ In fact, substantial X-ray structural evidence suggests that this event occurs by a volume conserving bicycle pedal motion^{1a,14,15} involving a reorientation of the central imine/enamine atoms (Figure 1b). One strategy to facilitate this process takes advantage of bulky substituents that twist the aromatic rings out of plane and generate some free volume in the lattice.¹⁵ Considering simple alternatives and based on our experience in the field of crystalline molecular rotors,¹⁶ we recognized that solid-state photochromism in SAs may be deliberately enabled by engineering crystals that allow the full rotation of the hydroxyl-containing ring (Figure 1a). In analogy with crystalline molecular rotor **1**¹⁷ in Figure 2, which

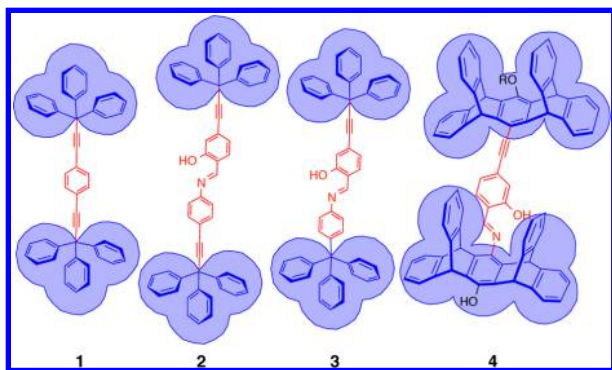


Figure 2. Phenylene molecular rotor **1** along with SA modified rotors **2**, **3**, and **4** (R = hexyl) with structures intended to facilitate the rotation of the phenol ring so that it can form the colored *trans*-keto form.

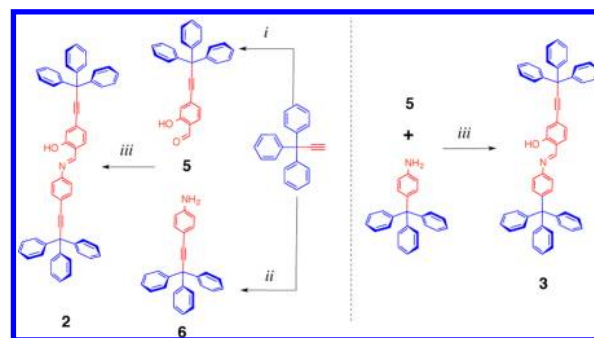
has a phenylene rotator shielded by two trityl groups acting as the stator, we decided to explore analogous structures with the two SA rings shielded by a bulky framework (Figures 1a and 2).

Using this basic design, we have confirmed the solid state photochromism of salicylidene aniline-bearing structures **2**, **3**, and **4** (Figure 2). Evidence that rotation of the phenol ring is possible was obtained by measuring the rotational dynamics of an isomorphous crystal of a *d*₄-labeled Schiff base analogue of **3** where the hydroxyl group had been removed (see below).

■ SYNTHESIS AND CHARACTERIZATION

The SA molecular rotors **2** and **3** were obtained by the convergent strategy shown in Scheme 1. For the synthesis of **2**, samples of tritylacetylene were converted into the salicylaldehyde half molecular rotor **5** using commercial 4-bromo-2-hydroxybenzaldehyde and standard Sonogashira conditions.¹⁸ Compound **6** was obtained in a similar manner from the same alkyne and 4-bromoaniline, and the desired SA **2** was prepared in 73% yield by condensation of **5** and **6**. Compound **3** was obtained by condensation of commercial 4-amino-tetraphenylmethane with SA **5** in 89% yield. The ¹H NMR spectra of **2** and **3** have the characteristic signals of the aldimine hydrogens with chemical shifts of 8.60 and 8.62 ppm, respectively, and those of the phenol hydrogens at 13.21 and 13.37 ppm. Their corresponding ¹³C NMR spectra showed signals of the aromatic hydroxyl-bearing carbon at 160.8 ppm for both compounds, and the imine carbons at 161.8 and 161.5 ppm. Four signals in the range of 84 and 97 ppm in the case of **2** correspond to the

Scheme 1^a

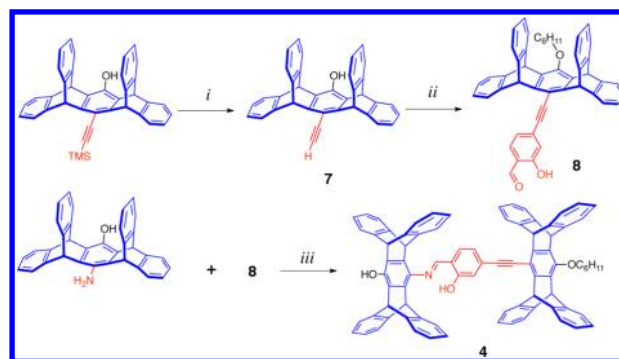


^aReaction conditions: (i) 4-bromo-2-hydroxybenzaldehyde, Pd(PPh₃)₄, CuI, diisopropylamine, benzene, reflux 8 h; (ii) 4-bromoaniline, Pd(PPh₃)₄, CuI, diisopropylamine, benzene, reflux 48 h; (iii) 4 Å molecular sieves, toluene, reflux 20 h.

two distinct alkynes the molecule. Accordingly, only two signals at 84.8 and 98.4 are observed for **3**. Two signals at 56.17 and 56.20 ppm correspond to the two quaternary trityl carbon atoms in the case of **2**, while the corresponding values in the case of **3** are 56.2 and 64.8 ppm. These assignments were corroborated in the case of **2** by analysis of a 2D HMBC spectrum. The FTIR spectra of solids **2** and **3** have a very broad signal that spans from ca. 3400–2600 cm⁻¹ attributed to the O–H stretch and a signal at ca. 1620 cm⁻¹ assigned to the C=N functionality, in agreement with the *cis*-enol form.¹⁹

As shown in Scheme 2, the synthesis of the bis-pentiptycene derivative **4** was completed by condensation of the known 6-

Scheme 2^a

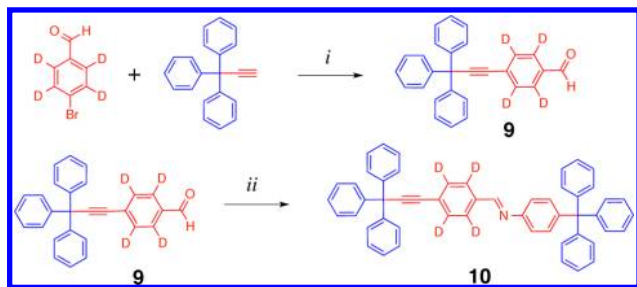


^aReaction conditions: (i) potassium carbonate, 1-bromohexane, dry acetone, reflux 12 h, followed by TBAF, THF at 50 °C for 0.5 h; (ii) 4-bromo-2-hydroxybenzaldehyde, Pd(PPh₃)₄, CuI, diisopropylamine, benzene, reflux 48 h; (iii) 4 Å molecular sieves, toluene, reflux 20 h.

amino-13-hydroxy-pentiptycene²⁰ with salicylaldehyde pentiptycene **8** with a yield of 74%, as shown in Scheme 2. This synthesis started with the preparation of compound **8** by Sonogashira coupling of commercial 4-bromo-2-hydroxybenzaldehyde with the pentiptycene derivative **7**. Precursor **7** was formed in two steps starting from the TMS-protected alkyne pentiptycene,²¹ which was alkylated using 1-bromohexane to increase its solubility. The ¹H NMR spectrum of compound **4** showed that the protons on the bridgehead carbons of the different pentiptycene halves were resolved with chemical shifts at 5.62, 5.74, 5.75, and 5.94 ppm, each signal integrating for two protons to a total of eight bridgehead protons. All the ¹H and ¹³C NMR signals from the central SA chromophore were

consistent with those described above for compounds **2** and **3**. Similarly, in addition to the stretching bands assigned to the SA unit, the IR spectrum of **4** has two broad phenolic O–H bands in the 3500–3100 cm^{-1} region, corresponding to the OH of the pentiptycene portion and the *cis*-enol form.

Finally, in order to explore the rotational dynamics of the trityl group-shielded SA phenolic ring (ring A in Figure 1), we synthesized d_4 -labeled compound **10** by condensing 4-amino-tetraphenylmethane with deuterated aldehyde **9** in 62% yield (Scheme 3). The spectroscopic properties of this model

Scheme 3^a

^aReaction conditions: (i) 4-bromo-2-hydroxybenzaldehyde, Pd-(PPh₃)₄, CuI, diisopropylamine, benzene, reflux 8 h; (ii) 4 Å molecular sieves, toluene, reflux 20 h.

compound were in good agreement with expectations, including the degree of deuterium labeling, which also was confirmed by high-resolution mass spectrometry. Satisfyingly, as described below, the powder X-ray diffraction of imine **10** is essentially identical to that of the analogous SA rotor **3**, which is indicative of a nearly identical packing structure.

CRYSTALLIZATION STUDIES AND SINGLE CRYSTAL X-RAY DIFFRACTION ANALYSES

Crystallization studies for compounds **2**–**4** were carried out at room temperature using different dry solvents and solvent mixtures. The selection of solvents was based on sample solubility and on the stability of the imine groups. Samples were soluble in chloroform, dichloromethane, toluene, and xylenes, but their solubility was low in acetonitrile and in hexanes. Traces of water in methanol and ethanol caused the slow hydrolysis of **2**, and these solvents were avoided. In a typical experiment, ca. 15 mg of the selected compound was placed in a small glass vial, dissolved with the appropriate solvent or solvent mixture (ca. 1 mL), and capped. Samples were monitored regularly until the appearance of the first crystals, which were taken out of the solution and immediately covered with oil to prevent the escape of solvent of crystallization. X-ray data was collected at 100(2) K, and selected crystallographic parameters for all three compounds are compiled in the Supporting Information.

Small crystals of **2** were obtained by slow evaporation from dichloromethane, and their structure was solved in the triclinic space group $P\bar{1}$ with one SA molecular rotor and one highly disordered solvent molecule per asymmetric unit. The crystals became opaque when exposed to open air, suggesting a rapid desolvation process. The molecular structure showed disorder in the salicylidene aniline portion, which was particularly evident in the C–OH and C=N groups, which were disordered over two positions related by a 180° rotation over an axis perpendicular to the molecular axis (Figure 3) with an

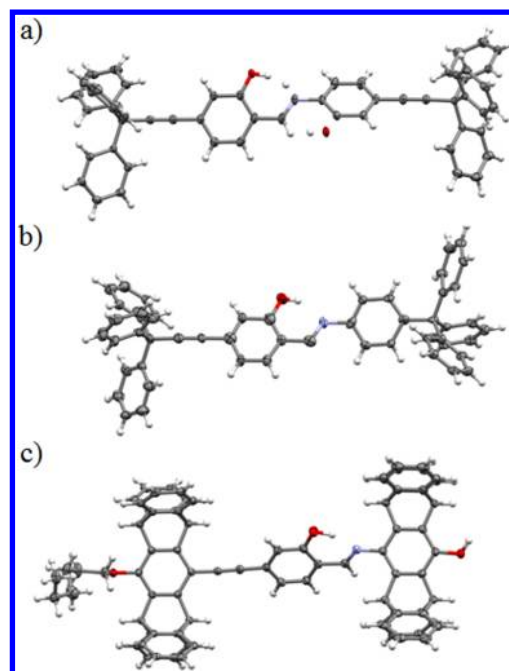


Figure 3. (a) Molecular structure of SA molecular rotor **2** showing a superposition of two disordered positions with occupancy of 56:44 and the central phenyl rings adopting a twisted conformation. (b) One of the two disordered positions with occupancy 87% of **3** that crystallizes with one cyclohexane molecule (not shown). (c) Molecular structure of the solvate of pentiptycene SA molecular rotor **4** obtained from acetonitrile (solvent molecules omitted). All the thermal ellipsoids are shown at 50% probability.

occupancy 56:44. As a result of the disorder, a confirmation of the *cis*-enol previously determined by spectroscopic means was not possible. The C_{Ar}–OH and the C_{Ar}–H bond distances displayed an average 1.289(2) Å, instead of values of ca. 1.35 and 0.95 Å expected for phenolic and C–H bonds, respectively.^{14a} The Schiff base has a conformation where the two aromatic rings in the salicylidene aniline portion are not planar, with the angle between mean planes slightly larger than 45°; this twisted conformation is characteristic of compounds with photochromic behavior,²² which in the case of compound **2** was explored by diffuse reflectance in the solid state, as discussed in the following sections. The packing structure shows the lattice-forming trityl groups guiding the crystallization in a displaced parallel arrangement by adopting a Ph...Ph interaction known as a 4-fold phenyl embrace or quadruple phenyl embrace (QPE),²³ with two phenyl rings showing edge-to-face propagating interactions with neighboring trityl groups. Some interdigitation occurs between adjacent molecules such that the trityl group of adjacent molecules are in close proximity with the salicylidene aniline component (Figure 4a).

Crystals of SA molecular rotor **3** were obtained from a mixture of cyclohexane/dichloromethane. Small single crystals had a tendency to degrade when exposed to ambient conditions. X-ray diffraction data was solved in the monoclinic system, space group C2 with one molecule of cyclohexane per molecule of **3**. Structural analysis was complicated by the disorder of the salicylidene aniline part over two alternate positions related by 180° over an axis perpendicular to the molecular axis with an occupancy of 87:13. In our model, only the major component was refined anisotropically and is shown in Figure 3b. In this structure, the central aromatic rings adopt a

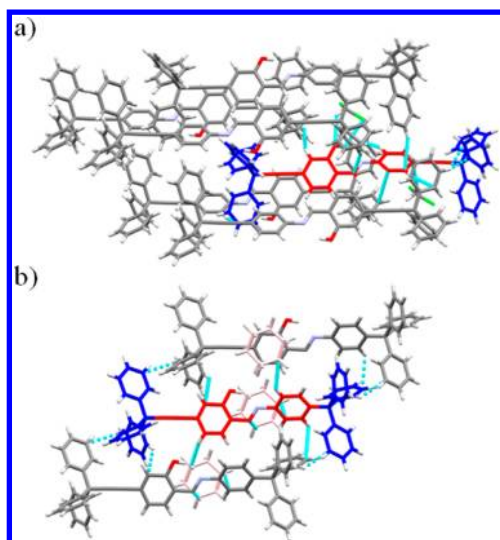


Figure 4. Comparison of the crystal packing of compounds **2** and **3** showing the parallel array of molecules along close contacts (light blue lines) with the salicylidene aniline portion (highlighted in red). (a) Compound **2** showing four intermolecular contacts of the adjacent trityl groups over the aniline ring and two over the salicylidene ring. (b) In compound **3**, the aniline portion has three close contacts, two of them with the loosely bound solvent highlighted in pink, while the salicylidene ring has two (one with solvent).

more planar conformation with an angle between mean aromatic planes close to 23° . Packing interactions between adjacent trityl groups favored a herringbone-like packing of aromatic molecules, where molecules of compound **3** crystallize in perpendicular layers with the molecular axis roughly parallel to the *b,c*-crystallographic plane. Compared with compound **2**, the salicylidene aniline moiety in **3** shows fewer intermolecular interactions, mainly with the cyclohexane molecules in the lattice (Figure 4b).

Compound **4** showed the lowest solubility of all, and crystals obtained from dichloromethane or chloroform become opaque within seconds when exposed to air. Plates obtained by slow evaporation from a mixture of dichloromethane/acetonitrile were suitable for X-ray diffraction. Data were collected at 100(2) K and solved in the monoclinic space group $P2_1/c$. A considerable amount of highly disordered solvent was found within the cavity generated by the pentiptycene framework, which is well-known to form host–guest complexes.²⁴ In our model, five molecules of acetonitrile were found per molecule of **4**. In contrast to the molecular structures of compounds **2** and **3**, that of compound **4** did not present disorder of the salicylidene aniline moiety, with $C_{Ar}-OH$ and $C=N$ bond distances of 1.354(3) and 1.287(3) Å, respectively, indicating the presence of a *cis*-enol tautomer. The salicylidene rings adopt a twisted conformation with an angle between mean planes of 45.6° . In this array, the pentiptycene halves acquire a coplanar conformation, allowing adjacent molecules to aggregate in a head-to-head fashion forming parallel-displaced layers in a zigzag pattern (see Supporting Information). The rigid framework efficiently protects the inner part of the molecule by generating a relatively large cavity filled with acetonitrile.

SOLID STATE PHOTOCHROMISM

As mentioned, the 1H NMR, ^{13}C NMR, and IR spectra are consistent with the stable *cis*-enol as the predominant form. In order to determine the relative contributions of the *cis*-enol and

trans-keto forms of SA molecular rotors **2–4**, spectroscopic measurements were carried out using UV–vis diffuse reflectance before and after exposure to UV light.

Well-characterized polycrystalline powders were placed onto a barium sulfate plate and pressed, and their diffuse reflectance was measured before irradiation with 365 nm UV light for 15 min at 300 K.²⁵ After that, as illustrated in Figure 5 for the case

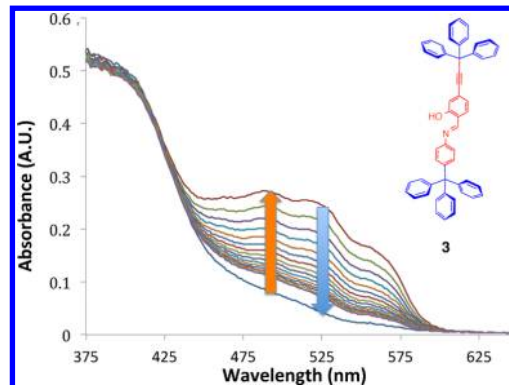


Figure 5. Optical absorption from the Kubelka–Monk function analysis of diffuse reflectance measurements of SA rotor **3** obtained immediately after irradiation with $\lambda = 365$ nm (orange arrow) and after various decay periods (blue arrow).

of compound **3**, diffuse reflectance measurements of the photogenerated *trans*-keto form were carried out over time scales that ranged from 6000 (ca. 1.6 h) to 50000 s (ca. 13.9 h). While a photochromic response was observed for all three samples, their increase in the visible absorption band was different; in the order $3 > 2 \gg 4$ (Table 1). The spectrum of

Table 1. Extent of Reaction, Lifetime of the *trans*-Keto Form, and Parameters That May Affect the Photochromism of the Three SA Rotors

	SA rotor 2	SA rotor 3	SA rotor 4
increase factor in <i>keto</i> form absorption after $h\nu^a$	1.69	4.5	1.06
lifetime T_1 (s)	174 ± 14	405 ± 2	1819 ± 472
lifetime T_2 (s)	1392 ± 71	1952 ± 13	16468 ± 1920
density, ρ [$Mg\ m^{-3}$]	1.271	1.208	1.216
near neighbors/number of solvent ^b	6/2	5/2	2/5

^aEquilibration attained after ca. 15 min irradiation at 365 nm.

^bNumber of atoms from neighboring molecules within a threshold of 3 Å. The distances for these close contacts can be found in the Supporting Information.

compound **2** is characterized by an absorption band that extends from ca. 270 to 450 nm with a λ_{max} at ca. 380 nm that can be assigned to the *cis*-enol. A weak shoulder in the range of 450–550 nm is assigned to the small equilibrium concentrations of the *cis*-keto form. Exposure to 365 nm UV light resulted in the growth of a broad band that extends up to 600 nm with a λ_{max} at ca. 475 nm, with an absorbance increased by a factor of 1.69 (Table 1) from 0.065 to 0.110 ± 0.003 . This band is assigned to the *trans*-keto form, which decays in a manner that can be described by a biexponential function with components having lifetimes of 174 ± 14 s and 1392 ± 71 s.

The solid state spectra obtained from compound **3** (Figure 5) were similar to those of **2**. Before irradiation, the spectrum

has a λ_{max} at 376 nm and a weak shoulder that extends to ca. 600 nm, which we tentatively assign, respectively, to the *cis*-enol and the *cis*-keto forms. Exposure to UV light resulted in the growth of a new broad, vibrationally resolved absorption band between ca. 400–600 nm with a 4.5-fold increase in absorbance from 0.060 to 0.270 ± 0.002 at 525 nm (Figure 5). The lifetime for **3** was also fit to a biexponential function, with a fast component of 405 ± 2 s and a slow component of 1952 ± 13 s. Solid samples of compound **4** showed a spectrum with a broad band between 275 and 450 nm and a λ_{max} at ca. 350 nm and weaker broad band that extends from 450 to 600 nm. Notably, irradiation with UV light resulted in a very small growth of the latter with a change in absorbance by a factor of only 1.06, from 0.240 to 0.255 ± 0.005 . The lifetime for **4** was fit with a biexponential function, with a fast component having a lifetime of 1820 ± 470 s and a slow component having a lifetime of 16470 ± 1920 s. The long wavelength absorbance and small photochromic response in the case of **4** is likely the result of electron donation by the hydroxyl group.²⁶

A potential correlation between crystal density or number of close neighbors in the lattice and the magnitude of the photochromic response observed is not evident. A clear distinction between compounds **2** and **3**, which have reasonably high responses, and compound **4**, which shows a very small variation, indicates the importance of electronic factors. It is worth noting that the lifetime of the *trans*-keto tautomers of compounds **2** and **3** are relatively short compared with those of other structures, in agreement with a molecular design intended to facilitate the rotations of the hydroxyl-bearing aromatic group.^{15c,27}

■ SOLID-STATE ^2H NMR

In order to support the suggested role for molecular rotation on the solid state photochromism of salicylidene anilines (Figure 1), we analyzed the rotation of a model Schiff base prepared with aldehyde analogue **9**, which lacks the *ortho*-hydroxyl group. Considering the relatively large photochromic response observed in the case compound **3**, we prepared analogue **10** with a deuterium-labeled aldimine ring (Scheme 3). We reasoned that removal of the hydroxyl group would be likely to result in a crystalline solid with a packing arrangement isomorphous to that of **3**. Gratifyingly, X-ray powder diffraction data corroborated this hypothesis (see Supporting Information), which allowed us to confirm that the shielding provided by the trityl framework would allow for the fast rotation of the aldimine. Without energetic contributions from the intramolecular hydrogen bond, we expected the rotational potential to be symmetric with equivalent sites related by 180° jumps. We selected a d_4 -labeled aldimine derivative because solid-state ^2H NMR is an ideal technique to probe the solid state dynamics of groups bearing C–D bonds.²⁸ Quadrupolar echo spectra acquired with static powdered samples as a function of temperature (ca. 100 mg) are expected to display changes in line shape that depend on the frequencies and trajectories of motion. In the case of 1,4-phenylene groups undergoing 180° rotations in crystalline environments, a very broad spectrum characteristic of static samples, known as a Pake pattern, can be obtained at sufficient low temperature.²⁹

Changes in the spectral line shape occur in predictable manner as a function of rotational exchange rates as the temperature increases. In practice, the experimental spectrum is simulated using a suitable dynamic model that includes a set of parameters that are characteristic of the molecules of interest.

Excellent simulation models developed by experts are currently available on the Internet.^{30,31} In the case of deuterated phenylenes, we consider (1) a quadrupolar coupling constant $\text{QCC} = 180$ kHz, (2) an asymmetry parameter $\eta = 0$, (3) the number of sites along a symmetric potential, which in this case is $n = 2$, (4) a value of $\alpha = 60^\circ$ for the cone angle made by the rotating C–D bond vector and the rotational axis, and (5) the frequency of exchange between sites.^{28,29} Spectral changes display a relatively high sensitivity in the intermediate regime between ca. 10^4 and 10^8 Hz. Slow exchanging ($<10^4$ Hz) and static samples are characterized by a symmetric spectrum with two intense peaks separated by ca. 130 kHz that are flanked by two outer shoulders that extend up to ca. 250 kHz.^{28,29} By contrast, the spectrum observed for rotational exchange in the fast exchange limit ($>10^8$ s⁻¹) consists of two peaks with a separation of only 32 Hz, tall shoulders that expand a width of ca. 125 kHz, and a second set of small peaks separated by ca. 155 kHz. Intermediate rotation frequencies lead to spectra whose appearance is between these.

As illustrated in Figure 6, ^2H NMR spectra obtained in the temperature range between 270 and 348 K display changes in

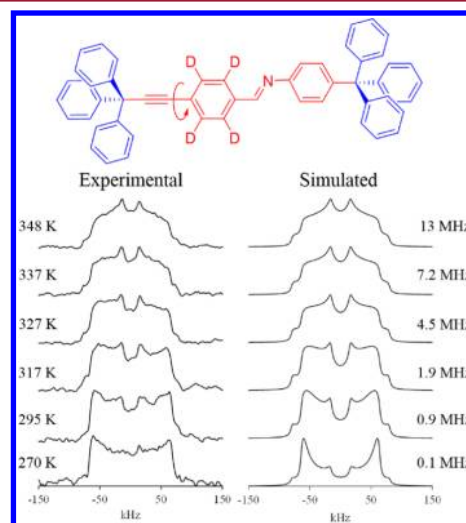


Figure 6. Experimental (left) and simulated (right) ^2H line shapes of model compound **10**. The experimental data was obtained at the temperatures indicated, and the simulated spectra were obtained with the program NMRweblab using the rotational exchange frequencies noted and the parameters listed in the text.

line shape with the intensity of the outer peaks decreasing and that of the inner peaks increasing, as expected for rotational motion within the 10^4 to 10^7 Hz range. The general features of the spectra and the changes observed as a function of temperature above 295 K were reasonably matched with a simulation model that assumes a Log-Gaussian distribution of rotational frequencies with a width $\sigma = 1.0$ centered in the range of 1.2–10 MHz.^{31,32} A Log-Gaussian distribution is indicative of a Gaussian distribution of activation energies,³² which is consistent with the orientationally disordered nature of the sample. Notably, the spectrum obtained at 270 K is poorly matched by a simulation carried out with values extrapolated from the other five data points and the frequency suggested should be considered as an upper limit. Although this disagreement may be due to the greater uncertainty of the data near the slow exchange regime, it may also arise from a temperature-dependent potential energy surface related to the

“softening” of the crystal within the corresponding temperature range.³³ Measurements at temperatures higher than 350 K did not cause significant changes in the spectra, indicating that rotation occurs with rates that are faster than the time scale of the ²H NMR experiment (fast exchange regime).

Using the experimental temperatures and the mean exchange frequencies of the simulations, we were able to construct an Arrhenius plot to determine the approximate activation energy (E_a) and pre-exponential factor (A) (Figure 7). While a value of

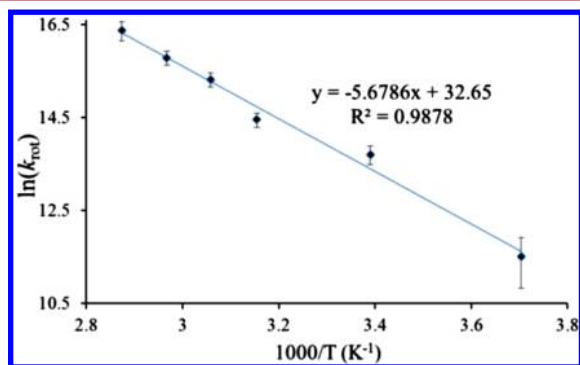


Figure 7. Arrhenius plot of **10** indicating a mean barrier to rotation of 11.2 kcal in the crystalline state.

$E_a = 11.2 \text{ kcal mol}^{-1}$ is in line with our design and expectations for the phenylene rotation, a pre-exponential factor $A = 1.5 \times 10^{14} \text{ s}^{-1}$ is greater than that expected for a phenylene rotator based on its moment of inertia.¹⁷ Notably, computational analysis of a model (*E*)-*N*-benzylideneaniline carried out at the B3LYP and M06 levels of theory by rotation of the phenyl–aldimine σ bond (Ph–C=N–) while the rest of the structure is allowed to minimize suggested barriers to rotation of 8.43 and 8.76 kcal/mol, respectively. These values suggest that the experimental barrier in the case of **10** may be largely determined by molecular electronic factors, rather than by steric barriers in the crystal lattice. Thus, recognizing that aldimine **10** is isomorphous with SA **3**, it is reasonable to conclude that rotation of the oxygen-bearing ring should not be significantly inhibited by nearest neighbors.

REACTION CAVITY ANALYSIS

Reactions in crystals require that the size and shape of the transition states, intermediates, and final products match well those of the reaction cavity determined by the boundary formed by the nearest neighbors of the reactant.³⁴ The relative preference of two competing products can be determined by measuring the root-mean-square deviation (RMSD) of the best overlap between each of their structures and that of the reactant, which is a measure of how well they would fit in the reaction cavity. Considering that the *trans*-keto forms in Figure 1 originating either from ring rotation or bicycle pedal motion are actually different structures, we decided to analyze the RMSD of their best overlap with the structure of the *cis*-enol, as shown in Figure 8. The structure of the *trans*-keto form was modeled by simple rotation of the oxygen-bearing ring. In contrast, the structure corresponding to the bicycle pedal mechanism was modeled by taking the coordinates of the salicylidene aniline portion of the crystal data for the *trans*-keto form shown by Harada et al. to occur by this mechanism^{14a} and attaching the bulky trityl and tritylethynyl groups. It has been shown that bicycle pedal motion requires not only the

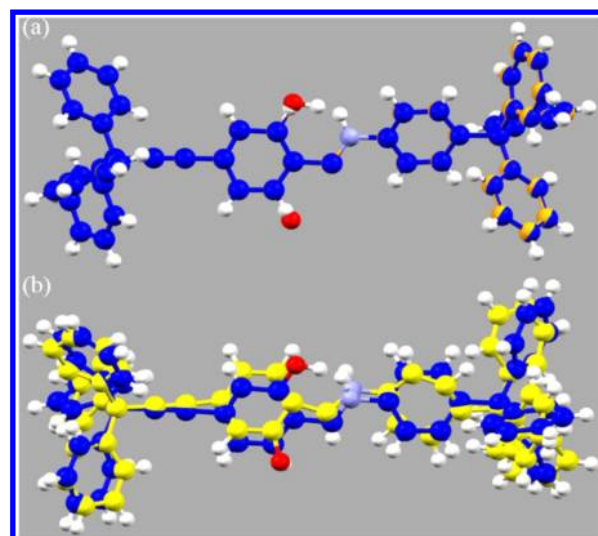


Figure 8. (a) Crystal structure of *cis*-enol **3** in blue superimposed on the *trans*-keto via 180° rotation in orange. (b) Crystal structure of *cis*-enol **3** in blue superimposed on the *trans*-keto via bicycle pedal functionalized to emulate **3** in yellow.

reorientation of the central C=N double bond but also a change in the direction of the two aromatic rings, which requires some motion of the trityl groups that are likely to act as anchors and prevent this motion. The RMSD³⁵ calculated for the ring rotation mechanism is only 3.3×10^{-5} and that for the bicycle pedal motion is 0.67. Both these values and inspection of Figure 8 indicate that the bicycle pedal mechanism requires significantly greater structural changes and should be more demanding than the 2-fold ring flip, supporting the latter as the preferred mechanism.

CONCLUSIONS

We have synthesized and fully characterized three molecular rotors with salicylidene aniline rotators encapsulated by bulky groups that generate a low density region for rotation of the oxygen-bearing aromatic group to rotate in the solid state. While all three SA molecular rotors generated the colored *trans*-keto tautomer upon irradiation with UV light, the extent of the photochromic reaction was significantly larger for the simpler SA chromophores **2** and **3** compared with the *para*-hydroxy substituted chromophore in molecular rotor **4**, which highlights the importance of electronic factors. In order to obtain evidence for a mechanism that involves the postulated ring rotation, we prepared and analyzed the rotational dynamics of molecular rotor **10**, an isotopically labeled deoxo-analogue of **3** that crystallizes in an isomorphous crystal structure. Using ²H NMR line shape analysis, we determined the ground state barrier for rotation of **10** to be 11.2 kcal/mol. Furthermore, a very small RMSD value for the best structural overlap between the starting *cis*-enol and the *trans*-keto form obtained by ring rotation suggest allowed solid state reactions. The evidence presented here strongly supports the use of crystal-engineered ring rotation as an alternative to bicycle pedal motion to obtain photochromic salicylidene anilines.

ASSOCIATED CONTENT

Supporting Information

Synthesis, analytical data, and experimental procedures and crystallographic data (CIF) for salicylidene aniline molecular

rotors 2, 3, and 4. This material is available free of charge via the Internet at <http://pubs.acs.org>.

AUTHOR INFORMATION

Corresponding Author

*E-mail: mgg@chem.ucla.edu.

Author Contributions

The manuscript was written through contributions of all authors.

Funding

This research was supported by NSF Grant DMR1101934.

Notes

The authors declare no competing financial interest.

REFERENCES

- (1) (a) Hadjoudis, E.; Mavridis, I. M. *Chem. Soc. Rev.* **2004**, *33*, 579. (b) Irie, M. *Chem. Rev.* **2000**, *100*, 1683. (c) Heinz Dürr, H., Bouas-Laurent, H., Eds., *Photochromism: Molecules and Systems*; Elsevier, Amsterdam, 2003.
- (2) (a) Castet, F.; Rodriguez, V.; Pozzo, J.-L.; Ducasse, L.; Plaquet, A.; Champagne, B. *Acc. Chem. Res.* **2013**, *46*, 2656. (b) Safin, D. A.; Robeyns, K.; Garcia, Y. *CrystEngComm* **2012**, *14*, 5523. (c) Delaire, J. A.; Nakatani, K. *Chem. Rev.* **2000**, *100*, 1817.
- (3) (a) Moorthy, J. N.; Mandal, S.; Mukhopadhyay, A.; Samanta, S. J. *Am. Chem. Soc.* **2013**, *135*, 6872. (b) Bruder, F.-K.; Hagen, R.; Rolle, T.; Weiser, M.-S.; Facke, T. *Angew. Chem., Int. Ed.* **2011**, *50*, 4552. (c) Feringa, B. L.; Jager, W. F.; Lange, B. De. *Tetrahedron* **1993**, *49*, 8267.
- (4) (a) Zhang, J.; Zou, Q.; Tian, H. *Adv. Mater.* **2013**, *25*, 378. (b) Natali, M.; Giordani, S. *Chem. Soc. Rev.* **2012**, *41*, 4010. (c) Byrne, R. J.; Stitzel, S. E.; Diamond, D. J. *Mater. Chem.* **2006**, *16*, 1332.
- (5) (a) Yamada, M.; Kondo, M.; Mamiya, J. I.; Yu, Y. L.; Kinoshita, M.; Barrett, C. J.; Ikeda, T. *Angew. Chem., Int. Ed.* **2008**, *47*, 4986. (b) Commins, P.; Garcia-Garibay, M. A. *J. Org. Chem.* **2014**, *79*, 1611.
- (6) (a) Terao, F.; Morimoto, M.; Irie, M. *Angew. Chem., Int. Ed.* **2012**, *51*, 901. (b) Uno, K.; Niikura, H.; Morimoto, M.; Ishibashi, Y.; Miyasaka, H.; Irie, M. *J. Am. Chem. Soc.* **2011**, *133*, 13558. (c) Fukaminato, T.; Doi, T.; Tamaoki, N.; Okuno, K.; Ishibashi, Y.; Miyasaka, H.; Irie, M. *J. Am. Chem. Soc.* **2011**, *133*, 4984.
- (7) (a) Klajn, R. *Chem. Soc. Rev.* **2014**, *43*, 148. (b) Liu, F.; Morokuma, K. *J. Am. Chem. Soc.* **2013**, *135*, 10693. (c) Harada, J.; Kawazoe, Y.; Ogawa, K. *Chem. Commun.* **2010**, *46*, 2593.
- (8) (a) Bushuyev, O. S.; Tomberg, A.; Fris, T.; Barrett, C. J. *J. Am. Chem. Soc.* **2013**, *135*, 12556. (b) Kolpak, A. M.; Grossman, J. C. *Nano Lett.* **2011**, *11*, 3156.
- (9) (a) Koshima, H.; Matsuo, R.; Matsudomi, M.; Uemura, Y.; Shiro, M. *Cryst. Growth Des.* **2013**, *13*, 4330. (b) Harada, J.; Nakajima, R.; Ogawa, K. *J. Am. Chem. Soc.* **2008**, *130*, 7085. (c) Amimoto, K.; Kawato, T. *J. Photochem. Photobiol., C* **2005**, *6*, 207.
- (10) Johmoto, K.; Sekine, A.; Uekusa, H. *Cryst. Growth Des.* **2012**, *12*, 4779.
- (11) Johmoto, K.; Sekine, A.; Uekusa, H.; Ohashi, Y. *Bull. Chem. Soc. Jpn.* **2009**, *82*, 50.
- (12) (a) Flynn, C. R.; Michl, J. *J. Am. Chem. Soc.* **1974**, *96*, 3280. (b) Migirdicyan, E.; Baudet, J. *J. Am. Chem. Soc.* **1975**, *97*, 7400.
- (13) (a) Cohen, M. D.; Schmidt, G. M. J.; Flavian, S. J. *Chem. Soc.* **1964**, 2041. (b) Bregman, J.; Leiserowitz, L.; Osaki, K. *J. Chem. Soc.* **1964**, 2086.
- (14) (a) Harada, J.; Uekusa, H.; Ohashi, Y. *J. Am. Chem. Soc.* **1999**, *121*, 5809. (b) Harada, J.; Ogawa, K. *J. Am. Chem. Soc.* **2001**, *123*, 10884.
- (15) (a) Kawato, T.; Koyama, H.; Kanatomi, H.; Tagawa, H.; Iga, T. *J. Photochem.* **1994**, *78*, 71. (b) Kawato, T.; Kanatomi, H.; Koyama, H.; Igarashi, T. *J. Photochem.* **1986**, *33*, 199. (c) Kawato, T.; Koyama, H.; Kanatomi, H.; Isshiki, M. *J. Photochem.* **1985**, *28*, 103.
- (16) (a) Vogelsberg, C. S.; Garcia-Garibay, M. A. *Chem. Soc. Rev.* **2012**, *41*, 1892. (b) Karlen, S. D.; Reyes, H.; Taylor, R. E.; Khan, S. I.; Hawthorne, M. F.; Garcia-Garibay, M. A. *Proc. Natl. Acad. Sci. U. S. A.* **2010**, *107*, 14973. (c) Khuong, T.-A. V.; Nuñez, J. E.; Godinez, C. E.; Garcia-Garibay, M. A. *Acc. Chem. Res.* **2006**, *39*, 413–422. (d) Garcia-Garibay, M. A. *Proc. Natl. Acad. Sci. U. S. A.* **2005**, *102*, 10793.
- (17) (a) Dominguez, Z.; Dang, H.; Strouse, M. J.; Garcia-Garibay, M. A. *J. Am. Chem. Soc.* **2002**, *124*, 2398. (b) Dominguez, Z.; Dang, H.; Strouse, J. M.; Garcia-Garibay, M. A. *J. Am. Chem. Soc.* **2002**, *124*, 7719.
- (18) Chinchilla, R.; Nájera, C. *Chem. Soc. Rev.* **2011**, *40*, 5084.
- (19) These samples were checked before and after irradiation; however, no additional IR stretches were observed.
- (20) Yang, J.; Ko, C. J. *Org. Chem.* **2006**, *71*, 844.
- (21) Long, T. M.; Swager, T. M. *J. Mater. Chem.* **2002**, *12*, 3407.
- (22) Johmoto, K.; Ishida, T.; Sekine, A.; Uekusa, H.; Ohashi, Y. *Acta Crystallogr.* **2012**, *B68*, 297.
- (23) (a) Scudder, M.; Dance, I. *J. Chem. Soc., Dalton Trans.* **1998**, 329–344. (b) Scudder, M.; Dance, I. *Dalton* **2000**, 2909. (c) Dance, I.; Scudder, M. *New J. Chem.* **1998**, *22*, 481. (d) Lacour, J.; Bernardinelli, G.; Russell, V.; Dance, I. *CrystEngComm* **2002**, *4*, 165. (e) Stopin, A.; Garcia-Garibay, M. A. *Cryst. Growth Des.* **2012**, *12*, 3792.
- (24) Mosca, L.; Koutník, P.; Lynch, V. M.; Zyryanov, G. V.; Esipenko, N. A.; Anzenbacher, P. *Cryst. Growth Des.* **2012**, *12*, 6104.
- (25) Although the thermochromism of 2, 3, and 4 was not analyzed in detail, visual inspection of the three samples in this study displayed changes in color when the temperature was close to the melting point. Compounds 2 and 3 turned orange at ca. 200 °C and orange/red above 250 °C. Compound 4 is the orange/yellow at room temperature and develops a deeper red above 200 °C.
- (26) Liang, Z.; Liu, Z.; Gao, Y. *Spectrochim. Acta A* **2007**, *68*, 1231.
- (27) (a) Robert, F.; Naik, A. D.; Tinant, B.; Robiette, R.; Garcia, Y. *Chem.—Eur. J.* **2009**, *15*, 4327. (b) Kawato, T.; Kanaotim, H.; Amimoto, K.; Koyama, H.; Shigemizu, H. *Chem. Lett.* **1999**, 47.
- (28) (a) Duer, M. J. *Introduction to Solid-State NMR Spectroscopy*; Blackwell Publishing, Oxford, 2004. (b) Hoatson, G. L.; Vold, R. L. *NMR: Basic Princ. Prog.* **1994**, *32*, 1. (c) Mantsch, H. H.; Saito, H.; Smith, I. C. P. *Progr. NMR Spectrosc.* **1977**, *11*, 211.
- (29) Karlen, S. D.; Garcia-Garibay, M. A. *Top. Curr. Chem.* **2006**, *262*, 179.
- (30) Macho, V.; Brombacher, L.; Spiess, H. W. *Appl. Magn. Reson.* **2001**, *20*, 405.
- (31) NMR WebLab. <http://weblab.mpip-mainz.mpg.de/cgi-bin/weblab45/weblab.pl?weblab=init&version=4.5>, accessed March 22, 2014.
- (32) (a) Schmidt, C.; Kuhn, J.; Spiess, H. W. *Prog. Colloid Polym. Sci.* **1985**, *71*, 71. (b) Fischer, E. W.; Hellmann, G. P.; Spiess, H. W.; Hörth, F. J.; Gearius, U.; Wehrle, M. *Makromol. Chem. Suppl.* **1985**, *12*, 189.
- (33) Very large pre-exponential factors for rotation have been observed also for glassy samples above the glass transition temperature: Vogelsberg, C. S.; Bracco, S.; Beretta, M.; Comotti, C.; Sozzani, P.; Garcia-Garibay, M. A. *J. Phys. Chem. B* **2012**, *116*, 1623.
- (34) Cohen, M. D. *Angew. Chem., Int. Ed.* **1975**, *14*, 386.
- (35) The structural similarities between the *cis*-enol and the *trans*-keto form obtained by either ring rotation or bicycle pedal motion were determined by comparing the RMSD measurements of the structures for each pair using Mercury 3.3.